Rock and Soil Mechanics 2025 46(10): 3315−3328 ISSN 1000−7598
https: //doi.org/10.26599/RSM.2024.94300571 journal homepage: rocksoilmech.whrsm.ac.cn

Identification of consolidation model parameters using spatiotemporally varying pore water pressure measurements

ZHAN Run-tao[1, 2], YIN Xiao-meng[1, 3]

1. College of Architecture and Civil Engineering, Xinyang Normal University, Xinyang, Henan 464000, China
2. Henan Unsaturated Soil and Special Soil Engineering Technology Research Center, Xinyang Normal University, Xinyang, Henan 464000, China
3. School of Civil Engineering and Architecture, Hubei University of Arts and Science, Wuhan, Hubei 441053, China

Abstract: The study applies the least squares technique in conjunction with a series of spatiotemporally varying pore water pressure measurements to identify the geotechnical parameters of consolidation models. Firstly, a least squares function for pore water pressure, incorporating both temporal and spatial coordinates, is developed. Subsequently, a new Jacobian matrix is constructed to accommodate any number of temporal and spatial measurements. Using Taylor series expansion, the iterative equations for the Gauss-Newton, Levenberg, Marquardt, and Nielsen methods are derived. The proposed methods are validated using two numerical examples. In Case 1, the consolidation coefficient of Terzaghi's model is identified. Comparative analysis reveals that all four methods converge to the correct solution, although the Marquardt method converges more slowly. In Case 2, the coordinates of a point source in a two-dimensional fluid-saturated medium are identified using a poroelastic consolidation model. The Gauss-Newton method fails to accurately locate the point source, whereas the Nielsen method accelerates convergence but introduces multiple damping coefficient intervals and convergence values. The Marquardt method is more effective for point source identification. Additionally, the study highlights the importance of sensor placement and initial iteration coordinates for accurate point source identification. Both cases show that the proposed methods possess some noise resistance.

Keywords: consolidation; least square problem; Gauss-Newton method; Levenberg-Marquardt method; sensor layout

1 Introduction

Since Terzaghi's introduction of the one-dimensional consolidation theory in 1924 and Biot's extension to the three-dimensional theory in 1941, soil consolidation continues to be a crucial research topic in soil mechanics [1]. Relevant scholars had derived analytical solutions for pore water pressure in consolidation models under different boundaries and initial conditions. This paper considers an inverse problem of consolidation theory, using the least squares method and measured pore water pressure to determine the relevant geotechnical parameters in analytical solutions. In the geotechnical area, inverse analysis has been applied successfully because it generates a relatively objective determination of the parameters[2–5]. For an inverse formulation of the parameters identification, the variables are the model parameters. A way to find their values is to simulate several sets of laboratory or field tests and to minimize the differences between experimental and numerical values of stresses, strains, and water pore pressures. This type of problem can be divided into 2 categories: (1) deterministic techniques and (2) stochastic techniques[6]. One of deterministic technique is least squares method which leads to the gradient-based algorithms such as the Gauss-Newton method, the steepest descent method, and the Levenberg and Marquardt methods[7-8]. The gradient-based methods have been used for solving different geotechnical engineering problems, such as identifying soil parameters[9–11]. Luco et al.[12] estimated shear-wave velocities and material damping ratios by minimizing the difference between the experimental impedance functions obtained from forced vibration tests of the foundation and theoretical impedance functions obtained by an integral equation technique. Nagarajaiah et al.[13] developed a least squares technique with time segments to identify the piece-wise linear system properties, and the recorded displacements and velocities were employed to identify the periods and damping ratios. Samui et al.[14] adopt least square support vector machine (LSSVM) for determination of liquefactions susceptibility of soil based on standard penetration test data. Wu et al.[15] obtained parameters for heat generation based on the least squares method and the Levenberg-Marquardt (LM) algorithm, and input data is temperature. Bao et al.[16] applied the least squares method to determine the consolidation coefficient of Terzaghi's model, utilizing specimen compression and time as input data. By studying the literatures about damped least square methods published in recent years, Xiao et al.[17] summarized and analyzed the improvement strategies of damped least square methods. Recently, Raissi et al.[18] introduced physics-informed neural networks (PINNs), a framework for incorporating partial differential equation (PDE) constraints into deep learning using automatic differentiation. Bekele[19] employed PINNs to determine the

Received: 10 October 2024 Accepted: 9 June 2025
This work was supported by the National Natural Science Foundation of China (41807240) and the Nature Science Foundation of Hubei Province (2023AFB607).
First author: ZHAN Runtao, male, born in 1977, PhD, lecturer, focusing on inverse problem in geotechnical engineering and soil-structure interaction.
E-mail: zrt@xynu.edu.cn

consolidation coefficient in Terzaghi's problem. Amini et al.[20] validated the proposed inverse-modeling PINNs approach on Terzaghi's isothermal consolidation problem, Barry-Mercer's injection-production problem, and no-isothermal consolidation of an unsaturated soil layer. Gong et al.[21] applied PINNs to predict the consolidation coefficients in a layered consolidation model. As discussed in Karniadakis et al.[22] there are multiple bottlenecks associated with PINNs, including the training time of PINNs forward solvers compared to classical methods and their applicability to couple nonlinear problems.

Pore water pressure during the soil consolidation process is a special measurement, varying both temporally and spatially. Measuring pore water pressure is crucial in clarifying the hydrogeological conditions and ensuring safety in geotechnical engineering projects. Pore water pressure sensors are widely used in geotechnical applications such as landslides and soil consolidation and settlement[23-24]. How to account for the time and spatial variables in pore water pressure function within the least squares method, as well as the number of time and spatial points in iterative equations, is a topic worthy of investigation in the inverse problem of consolidation theory. Previous research has rarely addressed this issue. In this study, we develop an original Jacobi matrix that allows for the identification of relevant geotechnical parameters.

This study aims to identify geotechnical parameters in analytical solutions to consolidation equations using the least squares technique and measurements of pore water pressure varying both temporally and spatially. The first step is transforming the parameter identification problem into a least squares problem. The pore water pressure measurements in the least squares function are obtained by employing well-established analytical solutions. Subsequently, this study categorizes the pore water pressure function into three components: the parameters to be identified, the location coordinates, and the test time. The derivation of the iteration equations for the Gauss-Newton, Levenberg, Marquardt, and Nielsen methods is presented. Additionally, conventional research on iterative equations often utilizes a Jacobi matrix that is square, necessitating equal numbers of rows and columns. This constraint requires that the number of sampled time and spatial points meets specific conditions, which can complicate practical applications. In contrast, this study introduces a novel Jacobi matrix that is non-square, thereby accommodating any combination of measurement locations and time points and effectively identifying the associated parameters. Finally, the effectiveness of the proposed strategy is demonstrated by two numerical examples.

2 Computational models and the least squares method

We study the problem of determining geotechnical parameters using temporally and spatially varying pore pressure measurements through two classical soil consolidation models.

The first case involves identifying the consolidation coefficient of the classical Terzaghi one-dimensional consolidation model. To effectively apply consolidation theory in practice, determining the consolidation coefficient is essential. Several methods for calculating this coefficient have been proposed by some scholars[1]. Zhang et al.[25] evaluated the coefficient of consolidation using the relationship between primary consolidation settlement and its velocity. Bao et al.[16] employed the least squares method to compute the consolidation coefficient. Bao et al.[26] also calculated the consolidation coefficient using a genetic algorithm. The measurements from the aforementioned study focused on soil compression. This paper proposes a new method for evaluating the consolidation coefficient based on pore water pressure measurements and damped least squares method, thereby highlighting the potential application of pore water pressure sensors in engineering to assess the degree of consolidation.

The second case aims to identify the coordinates of a point source in the two-dimensional Barry–Mercer poroelastic consolidation model. The poroelastic equations were first derived by Biot[27] studying with the consolidation of soils. Barry et al.[28] derived analytical solutions for the time-dependent pore pressure caused by a point source within a finite rectangular poroelastic medium and the pore pressure field conforms to the first-type boundary conditions. Li et al.[29] derived analytical solutions when the pore water pressure field satisfies the second-type boundary conditions. These studies are applicable to incompressible porous media. Li et al.[30] derived an analytical solution for the finite 2-D compressible poroelastic media resulting from a point source. Li et al.[31] also investigated the time-dependent hydromechanical behavior of a finite two-dimensional fluid-saturated poroelastic medium caused by a point source. It is noted that the studies above on the point source problem are based on Biot's poroelasticity consolidation equations and boundary conditions in order to obtain analytical solutions of pore water pressure. In the paper, we consider the inverse problem of identifying the source point in Barry-Mercer consolidation model using pore water pressure measurements and damped least squares method.

The least squares method arises in the context of finding the correct solution to a linear or nonlinear system of equations by minimizing the objective, expressed as the sum of the squares of the errors between the model function and a set of data points and creating a recursive equation. In order to reduce the influence of errors in the observations, one would then like to use a greater number of measurements than the number of unknown parameters in the model. The result is an overdetermined linear system of equations to be solved[32].

In order to fit the measured values of the pore water pressure sensors, it is customary to minimize the sum of

squares of the errors between the $(l+1)$th iteration values of pore water pressure $p(\boldsymbol{\eta}^{(l+1)};\xi_i;t_j)$ and measured values $\bar{p}(\xi_i;t_j)$:

$$F\left(\boldsymbol{\eta}^{(l+1)};\xi_i;t_j\right)=\frac{1}{2}\sum_{j=1}^{J}\sum_{i=1}^{I}\left[p(\boldsymbol{\eta}^{(l+1)};\xi_i;t_j)-\bar{p}(\xi_i;t_j)\right]^2 \tag{1}$$

where $F(\cdot)$ is least square function; ξ_i denotes the sensor location's coordinates; t_j the test time; I is the total number of pore water pressure sensors; J is the total time point of the test; l is the number of iterations; at location i and time j, $p(\boldsymbol{\eta}^{(l+1)};\xi_i;t_j)$ represents the $(l+1)$th iteration value and $\bar{p}(\xi_i;t_j)$ represents the measurement of pore water pressure, $\boldsymbol{\eta}$ is a vector that contains the parameters that need to be identified.

Using the Taylor series expansion for $p(\boldsymbol{\eta}^{(l+1)};\xi_i;t_j)$, Eq.（1） becomes

$$F\left(\boldsymbol{\eta}^{(l+1)};\xi_i;t_j\right)=\frac{1}{2}\sum_{j=1}^{J}\sum_{i=1}^{I}\left[p(\boldsymbol{\eta}^{(l)};\xi_i;t_j)+\frac{\partial p(\boldsymbol{\eta}^{(l)};\xi_i;t_j)}{\partial\boldsymbol{\eta}^{(l)}}\Delta\boldsymbol{\eta}^{(l)}-\bar{p}\left(\xi_i;t_j\right)\right]^2 \tag{2}$$

where $\boldsymbol{\eta}^{(l+1)}=\boldsymbol{\eta}^{(l)}+\Delta\boldsymbol{\eta}^{(l)}$.

The necessary condition for requirement that $F(\boldsymbol{\eta}^{(l+1)};\xi_i;t_j)$ be minimal is

$$\frac{\partial F\left(\boldsymbol{\eta}^{(l+1)};\xi_i;t_j\right)}{\partial\boldsymbol{\eta}^{(l)}}=\sum_{j=1}^{J}\sum_{i=1}^{I}\left[p(\boldsymbol{\eta}^{(l)};\xi_i;t_j)-\bar{p}\left(\xi_i;t_j\right)+\frac{\partial p(\boldsymbol{\eta}^{(l)};\xi_i;t_j)}{\partial\boldsymbol{\eta}^{(l)}}\Delta\boldsymbol{\eta}^{(l)}\right]\times\left[\frac{\partial p(\boldsymbol{\eta}^{(l)};\xi_i;t_j)}{\partial\boldsymbol{\eta}^{(l)}}+\frac{\partial}{\partial\boldsymbol{\eta}^{(l)}}\left(\frac{\partial p(\boldsymbol{\eta}^{(l)};\xi_i;t_j)}{\partial\boldsymbol{\eta}^{(l)}}\Delta\boldsymbol{\eta}^{(l)}\right)\right]=0 \tag{3}$$

where $\dfrac{\partial}{\partial\boldsymbol{\eta}^{(l)}}(\cdot)=\dfrac{\partial}{\partial\boldsymbol{\eta}}(\cdot)\Big|_{\boldsymbol{\eta}=\boldsymbol{\eta}^{(l)}}$.

Omitting higher-order items leads to:

$$\sum_{j=1}^{J}\sum_{i=1}^{I}\left[p(\boldsymbol{\eta}^{(l)};\xi_i;t_j)-\bar{p}(\xi_i;t_j)+\frac{\partial p(\boldsymbol{\eta}^{(l)};\xi_i;t_j)}{\partial\boldsymbol{\eta}^{(l)}}\Delta\boldsymbol{\eta}^{(l)}\right]\times\frac{\partial p(\boldsymbol{\eta}^{(l)};\xi_i;t_j)}{\partial\boldsymbol{\eta}^{(l)}}=0 \tag{4}$$

The Eq.（4） can be rewritten in matrix form:

$$\boldsymbol{A}^{\mathrm{T}}\left(\boldsymbol{\eta}^{(l)};\xi_i;t_j\right)\left[p(\boldsymbol{\eta}^{(l)};\xi_i;t_j)-\bar{p}(\xi_i;t_j)\right]+\boldsymbol{A}^{\mathrm{T}}\left(\boldsymbol{\eta}^{(l)};\xi_i;t_j\right)\boldsymbol{A}\left(\boldsymbol{\eta}^{(l)};\xi_i;t_j\right)\Delta\boldsymbol{\eta}^{(l)}=0 \tag{5}$$

According to Eq.（5）, it is evident that

$$\Delta\boldsymbol{\eta}^{(l)}=-\left[\boldsymbol{A}^{\mathrm{T}}\left(\boldsymbol{\eta}^{(l)};\xi_i;t_j\right)\boldsymbol{A}\left(\boldsymbol{\eta}^{(l)};\xi_i;t_j\right)\right]^{-1}\times\boldsymbol{A}^{\mathrm{T}}\left(\boldsymbol{\eta}^{(l)};\xi_i;t_j\right)\left[p(\boldsymbol{\eta}^{(l)};\xi_i;t_j)-\bar{p}(\xi_i;t_j)\right] \tag{6}$$

where A is the Jacobian matrix and can be written as

$$\boldsymbol{A}(\boldsymbol{\eta}^{(l)};\xi_i;t_j)=\begin{bmatrix}\frac{\partial p(\boldsymbol{\eta}^{(l)};\xi_1;t_1)}{\partial\eta_1^{(l)}} & \frac{\partial p(\boldsymbol{\eta}^{(l)};\xi_1;t_1)}{\partial\eta_2^{(l)}} & \cdots & \frac{\partial p(\boldsymbol{\eta}^{(l)};\xi_1;t_1)}{\partial\eta_K^{(l)}}\\ \frac{\partial p(\boldsymbol{\eta}^{(l)};\xi_1;t_2)}{\partial\eta_1^{(l)}} & \frac{\partial p(\boldsymbol{\eta}^{(l)};\xi_1;t_2)}{\partial\eta_2^{(l)}} & \cdots & \frac{\partial p(\boldsymbol{\eta}^{(l)};\xi_1;t_2)}{\partial\eta_K^{(l)}}\\ \cdots & \cdots & \cdots & \cdots\\ \frac{\partial p(\boldsymbol{\eta}^{(l)};\xi_1;t_J)}{\partial\eta_1^{(l)}} & \frac{\partial p(\boldsymbol{\eta}^{(l)};\xi_1;t_J)}{\partial\eta_2^{(l)}} & \cdots & \frac{\partial p(\boldsymbol{\eta}^{(l)};\xi_1;t_J)}{\partial\eta_K^{(l)}}\\ \cdots & \cdots & \cdots & \cdots\\ \frac{\partial p(\boldsymbol{\eta}^{(l)};\xi_I;t_1)}{\partial\eta_1^{(l)}} & \frac{\partial p(\boldsymbol{\eta}^{(l)};\xi_I;t_1)}{\partial\eta_2^{(l)}} & \cdots & \frac{\partial p(\boldsymbol{\eta}^{(l)};\xi_I;t_1)}{\partial\eta_K^{(l)}}\\ \frac{\partial p(\boldsymbol{\eta}^{(l)};\xi_I;t_2)}{\partial\eta_1^{(l)}} & \frac{\partial p(\boldsymbol{\eta}^{(l)};\xi_I;t_2)}{\partial\eta_2^{(l)}} & \cdots & \frac{\partial p(\boldsymbol{\eta}^{(l)};\xi_I;t_2)}{\partial\eta_K^{(l)}}\\ \cdots & \cdots & \cdots & \cdots\\ \frac{\partial p(\boldsymbol{\eta}^{(l)};\xi_I;t_J)}{\partial\eta_1^{(l)}} & \frac{\partial p(\boldsymbol{\eta}^{(l)};\xi_I;t_J)}{\partial\eta_2^{(l)}} & \cdots & \frac{\partial p(\boldsymbol{\eta}^{(l)};\xi_I;t_J)}{\partial\eta_K^{(l)}}\end{bmatrix}_{(IJ)\times K} \tag{7}$$

where $\boldsymbol{\eta}^{(l)}=[\eta_1^{(l)},\eta_2^{(l)},\cdots,\eta_K^{(l)}]$ and $\eta_1^{(l)},\cdots,\eta_K^{(l)}$ are geotechnical parameters to be identified; and K is the number of parameters to be identified.

Jacobian matrix $A(\boldsymbol{\eta}^{(l)};\xi_i;t_j)$ is an original matrix which accounts for the sensor location's coordinates ξ_i $(i=1,\cdots,I)$ and the test time t_j $(j=1,\cdots,J)$.

The error vector in Eq.（6） is

$$p(\boldsymbol{\eta}^{(l)};\xi_i;t_j)-\bar{p}(\xi_i;t_j)=\begin{bmatrix}p(\boldsymbol{\eta}^{(l)};\xi_1;t_1)-\bar{p}(\xi_1;t_1)\\ p(\boldsymbol{\eta}^{(l)};\xi_1;t_2)-\bar{p}(\xi_1;t_2)\\ \cdots\\ p(\boldsymbol{\eta}^{(l)};\xi_1;t_J)-\bar{p}(\xi_1;t_J)\\ \cdots\\ p(\boldsymbol{\eta}^{(l)};\xi_I;t_1)-\bar{p}(\xi_I;t_1)\\ p(\boldsymbol{\eta}^{(l)};\xi_I;t_2)-\bar{p}(\xi_I;t_2)\\ \cdots\\ p(\boldsymbol{\eta}^{(l)};\xi_I;t_J)-\bar{p}(\xi_I;t_J)\end{bmatrix}_{(IJ)\times 1} \tag{8}$$

Equation（6） is a variant of the Gauss-Newton method. According to Jacobian matrix Eq.（7）, coordinate and time variables can be taken in different numbers.

3 Levenberg – Marquardt methods

The Gauss-Newton method has fast local convergence on mildly nonlinear problems. However, it may not even be locally convergent on problems that are very nonlinear or have large residuals[32]. Levenberg[7] and Marquardt[8] suggested the damped Gauss-Newton methods for nonlinear least squares problems.

The unconstrained nonlinear least squares Eq.（2） can be rewritten to find a global minimizer of the sum of squares

of nonlinear functions:

$$F\left(\boldsymbol{\eta}^{(l+1)};\xi_i;t_j\right)=$$
$$\frac{1}{2}\sum_{j=1}^{J}\sum_{i=1}^{I}\left[p(\boldsymbol{\eta}^{(l)};\xi_i;t_j)+\frac{\partial p(\boldsymbol{\eta}^{(l)};\xi_i;t_j)}{\partial\boldsymbol{\eta}^{(l)}}\Delta\boldsymbol{\eta}^{(l)}-\bar{p}\left(\xi_i^{(l)};t_j\right)\right]^2$$
$$\text{s.t. }\frac{1}{2}\left(\left\|\boldsymbol{D}\Delta\boldsymbol{\eta}^{(l)}\right\|^2-r^2\right)=$$
$$\frac{1}{2}\left[\left\|\boldsymbol{D}\left(\boldsymbol{\eta}^{(l+1)}-\boldsymbol{\eta}^{(l)}\right)\right\|^2-r^2\right]\leqslant 0 \tag{9}$$

where the r is radius of the trust region and D is the weight matrix.

Equation (9) may be stated as

$$L\left(\boldsymbol{\eta}^{(l+1)};\xi_i;t_j\right)=$$
$$\frac{1}{2}\sum_{j=1}^{J}\sum_{i=1}^{I}\left[p(\boldsymbol{\eta}^{(l)};\xi_i;t_j)+\frac{\partial p(\boldsymbol{\eta}^{(l)};\xi_i;t_j)}{\partial\boldsymbol{\eta}^{(l)}}\Delta\boldsymbol{\eta}^{(l)}-\bar{p}\left(\xi_i^{(l)};t_j\right)\right]^2+$$
$$\mu\times\frac{1}{2}\left(\left\|\boldsymbol{D}\Delta\boldsymbol{\eta}^{(l)}\right\|^2-r^2\right) \tag{10}$$

where $L(\cdot)$ is Lagrangian function, μ is Lagrangian multiplier, which is also damping parameter; and $\|\cdot\|$ denotes the 2 norms.

The differentiation of the Eq.(10) leads to

$$\frac{\partial L\left(\boldsymbol{\eta}^{(l+1)};\xi_i;t_j\right)}{\partial\boldsymbol{\eta}^{(l)}}=$$
$$\sum_{j=1}^{J}\sum_{i=1}^{I}\left[p(\boldsymbol{\eta}^{(l)};\xi_i;t_j)+\frac{\partial p(\boldsymbol{\eta}^{(l)};\xi_i;t_j)}{\partial\boldsymbol{\eta}^{(l)}}\Delta\boldsymbol{\eta}^{(l)}-\bar{p}\left(\xi_i;t_j\right)\right]\times$$
$$\left[\frac{\partial p(\boldsymbol{\eta}^{(l)};\xi_i;t_j)}{\partial\boldsymbol{\eta}^{(l)}}+\frac{\partial}{\partial\boldsymbol{\eta}^{(l)}}\left(\frac{\partial p(\boldsymbol{\eta}^{(l)};\xi_i;t_j)}{\partial\boldsymbol{\eta}^{(l)}}\Delta\boldsymbol{\eta}^{(l)}\right)\right]+$$
$$\mu\boldsymbol{D}^{\mathrm{T}}\boldsymbol{D}\Delta\boldsymbol{\eta}^{(l)}=0 \tag{11}$$

Equation (11) can become by omitting higher-order items:

$$\sum_{j=1}^{J}\sum_{i=1}^{I}\left[p(\boldsymbol{\eta}^{(l)};\xi_i;t_j)-\bar{p}\left(\xi_i;t_j\right)+\frac{\partial p(\boldsymbol{\eta}^{(l)};\xi_i;t_j)}{\partial\boldsymbol{\eta}^{(l)}}\Delta\boldsymbol{\eta}^{(l)}\right]\times$$
$$\frac{\partial p(\boldsymbol{\eta}^{(l)};\xi_i;t_j)}{\partial\boldsymbol{\eta}^{(l)}}+\mu\boldsymbol{D}^{\mathrm{T}}\boldsymbol{D}\Delta\boldsymbol{\eta}^{(l)}=0 \tag{12}$$

Equation (12) can be rewritten in matrix form:

$$\boldsymbol{A}^{\mathrm{T}}\left(\boldsymbol{\eta}^{(l)};\xi_i;t_j\right)\left[p(\boldsymbol{\eta}^{(l)};\xi_i;t_j)-\bar{p}\left(\xi_i;t_j\right)\right]+$$
$$\left[\boldsymbol{A}^{\mathrm{T}}\left(\boldsymbol{\eta}^{(l)};\xi_i;t_j\right)\boldsymbol{A}\left(\boldsymbol{\eta}^{(l)};\xi_i;t_j\right)+\mu\boldsymbol{D}^{\mathrm{T}}\boldsymbol{D}\right]\Delta\boldsymbol{\eta}^{(l)}=0 \tag{13}$$

where $\boldsymbol{A}(\boldsymbol{\eta}^{(l)};\xi_i;t_j)$, $p(\boldsymbol{\eta}^{(l)};\xi_i;t_j)-\bar{p}(\xi_i;t_j)$ are given in Eqs.(7) and (8).

So the update rule is

$$\Delta\boldsymbol{\eta}^{(l)}=-\left[\mu\boldsymbol{D}^{\mathrm{T}}\boldsymbol{D}+\boldsymbol{A}^{\mathrm{T}}\left(\boldsymbol{\eta}^{(l)};\xi_i;t_j\right)\boldsymbol{A}\left(\boldsymbol{\eta}^{(l)};\xi_i;t_j\right)\right]^{-1}\times$$
$$\boldsymbol{A}^{\mathrm{T}}\left(\boldsymbol{\eta}^{(l)};\xi_i;t_j\right)\left[p(\boldsymbol{\eta}^{(l)};\xi_i;t_j)-\bar{p}(\xi_i;t_j)\right] \tag{14}$$

When the matrix $\boldsymbol{D}^{\mathrm{T}}\boldsymbol{D}$ is the identity matrix $\boldsymbol{I}$ and the update rule becomes the Levenberg method:

$$\Delta\boldsymbol{\eta}^{(l)}=-\left[\mu\boldsymbol{I}+\boldsymbol{A}^{\mathrm{T}}\left(\boldsymbol{\eta}^{(l)};\xi_i;t_j\right)\boldsymbol{A}\left(\boldsymbol{\eta}^{(l)};\xi_i;t_j\right)\right]^{-1}\times$$
$$\boldsymbol{A}^{\mathrm{T}}\left(\boldsymbol{\eta}^{(l)};\xi_i;t_j\right)\left[p(\boldsymbol{\eta}^{(l)};\xi_i;t_j)-\bar{p}\left(\xi_i;t_j\right)\right] \tag{15}$$

where small values of the damping parameter μ result in Gauss-Newton method (Eq.(6)) and large values of μ result in steepest descent method:

$$\Delta\boldsymbol{\eta}^{(l)}=-\frac{1}{\mu}\boldsymbol{A}^{\mathrm{T}}\left(\boldsymbol{\eta}^{(l)};\xi_i;t_j\right)\left[p(\boldsymbol{\eta}^{(l)};\xi_i;t_j)-\bar{p}(\xi_i;t_j)\right] \tag{16}$$

The damping parameter μ influences both the direction and the size of the step, and this leads us to make a method without a specific line search. If the l(th) iteration $\boldsymbol{\eta}^{(l)}$ is close to the exact solution $\boldsymbol{\eta}$, then the correct convergence of the Gauss-Newton method is obtained. The choice of initial μ value should be related to the size of the elements in Hessian matrix $\boldsymbol{H}=\boldsymbol{A}^{\mathrm{T}}\boldsymbol{A}$.

Marquardt improved Levenberg algorithm by replacing the identity matrix $\boldsymbol{I}$ in Levenberg original equations with the diagonal of the Hessian matrix $\boldsymbol{A}^{\mathrm{T}}\boldsymbol{A}$ (Marquardt method)[8]:

$$\Delta\boldsymbol{\eta}^{(l)}=-\left\{\mu\,\mathrm{diag}\left[\boldsymbol{A}^{\mathrm{T}}\left(\boldsymbol{\eta}^{(l)};\xi_i;t_j\right)\boldsymbol{A}\left(\boldsymbol{\eta}^{(l)};\xi_i;t_j\right)\right]+\right.$$
$$\left.\boldsymbol{A}^{\mathrm{T}}\left(\boldsymbol{\eta}^{(l)};\xi_i;t_j\right)\boldsymbol{A}\left(\boldsymbol{\eta}^{(l)};\xi_i;t_j\right)\right\}^{-1}\boldsymbol{A}^{\mathrm{T}}\left(\boldsymbol{\eta}^{(l)};\xi_i;t_j\right)\cdot$$
$$\left[p(\boldsymbol{\eta}^{(l)};\xi_i;t_j)-\bar{p}(\xi_i;t_j)\right] \tag{17}$$

Nielsen et al.[33-34] proposed an updating strategy for damping parameter μ based on Marquardt method so that it can avoid slowing down convergence (Nielsen method):

$$\left.\begin{array}{l}\text{if }\rho>0\\ \mu=\mu\max\left\{1/3,1-(2\rho-1)^3\right\},\nu=2\\ \text{else}\\ \mu=\mu\nu,\nu=2\nu\end{array}\right\} \tag{18}$$

where ρ is gain ratio and ν is a parameter with an initial value of 2.

The damping parameter μ can be updated and is controlled by gain ratio ρ:

$$\rho=\frac{F\left(\boldsymbol{\eta}^{(l)};\xi_i;t_j\right)-F\left(\boldsymbol{\eta}^{(l+1)};\xi_i;t_j\right)}{\left[\Delta\boldsymbol{\eta}^{(l)}\right]^{\mathrm{T}}\left\{\mu\Delta\boldsymbol{\eta}^{(l)}-\boldsymbol{A}^{\mathrm{T}}\left[p(\boldsymbol{\eta}^{(l)};\xi_i;t_j)-\bar{p}(\xi_i;t_j)\right]\right\}/2} \tag{19}$$

where $F\left(\boldsymbol{\eta}^{(l+1)};\xi_i;t_j\right)$ is given in Eq.(1).

4 Numerical examples

In this section, two cases are used to verify the effectiveness of the proposed methods. Case 1 is to identify

the consolidation coefficient in the Terzaghi's one-dimension consolidation model in Section 4.1. Case 2 is to identify the coordinates of the point source in a two-dimensional fluid saturated media based on Barry-Mercer's poroelastic model in Section 4.2.

4.1 Identification of the consolidation coefficient

Terzaghi[1] developed an analytical model for determining the degree of consolidation within soil at any time. Consider an open layer of the fine-grained saturated soil with thickness 2*d*, as shown in Fig.1. The upper and lower boundaries of the soil layer are assumed to be free-draining, the permeability of the soil adjacent to each boundary being very high compared to that of the soil. Water therefore drains from the center of the soil element to the upper and lower boundaries simultaneously, so that the drainage path length is *d*. The Terzaghi one-dimensional differential equation of consolidation is [1]

$$\frac{\partial p}{\partial t}=c_{\mathrm{v}}\frac{\partial^2 p}{\partial z^2} \tag{20}$$

where c_{v} is the coefficient of consolidation.

The boundary and initial conditions are

$p=p_0$ for $0\leqslant z\leqslant 2d$ when $t=0$;

$p=0$ for $z=0$ and $z=2d$ when $t>0$.

The analytical solution of pore water pressure to the Terzaghi's consolidation equation at depth z after time t is

$$p=\sum_{m=0}^{\infty}\left(\frac{2p_0}{M}\sin\frac{Mz}{d}\right)\exp\left(-\frac{c_{\mathrm{v}}tM^2}{d^2}\right) \tag{21}$$

where $M=\pi(2m+1)/2$; and p_0 is the initial value of excess pore water pressure and is a constant.

As shown in Fig.1, there are 2 coordinate variables and 3 time variables for identifying the consolidation coefficient. According to Eq.（7） and Eq.（8）, the Jacobian matrix $\boldsymbol{A}(\boldsymbol{\eta}^{(l)};\xi_i;t_j)$, the l(th) iteration pore water pressure values $p(\boldsymbol{\eta}^{(l)};\xi_i;t_j)$ and the measured values $\bar{p}\left(\xi_i;t_j\right)$ are

$$\boldsymbol{A}\left(\boldsymbol{\eta}^{(l)};\xi_i;t_j\right)=\frac{\partial p\left(c_{\mathrm{v}}^{(l)};z_i;t_j\right)}{\partial c_{\mathrm{v}}}= -\frac{2p_0}{d^2}\sum_{m=0}^{\infty}t_jM\left(\sin\frac{Mz_i}{d}\right)\exp\left(-\frac{c_{\mathrm{v}}^{(l)}t_jM^2}{d^2}\right) \tag{22}$$

$$p\left(\boldsymbol{\eta}^{(l)};\xi_i;t_j\right)=p(c_{\mathrm{v}}^{(l)};z_i;t_j)= \sum_{m=0}^{\infty}\left(\frac{2p_0}{M}\sin\frac{Mz_i}{d}\right)\exp\left(-\frac{c_{\mathrm{v}}^{(l)}t_jM^2}{d^2}\right) \tag{23}$$

$$\bar{p}(\xi_i;t_j)=p(z_i;t_j)= \sum_{m=0}^{\infty}\left(\frac{2p_0}{M}\sin\frac{Mz_i}{d}\right)\exp\left(-\frac{c_{\mathrm{v}}t_jM^2}{d^2}\right) \tag{24}$$

where $\boldsymbol{\eta}^{(l)}$ is a vector containing the parameter to be identified and $\boldsymbol{\eta}^{(l)}=[c_{\mathrm{v}}^{(l)}]$; and ξ_i is the sensor location's coordinate, $\xi_i=z_i$.

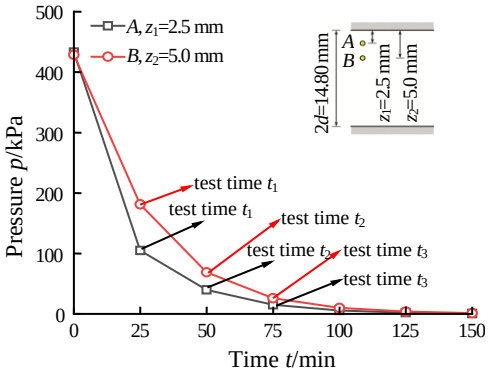


Fig.1 Layout of pore water pressure sensors and pore water pressure time history curves based on Terzaghi's model

The parameters of Eq.(21) are chosen on the basis of the values given in Example 4.3 of the literature [1].

(1) The initial excess pore water pressure p_0 =429 kPa and the consolidation coefficient c_{v} = 0.46 m^2/y = 0.858 6 mm^2/min. Initial iteration consolidation coefficient $c_v^{(1)}$ =0.1.

(2) Length of drainage path: d =7.4 mm. The arrangement of the pore water pressure sensors is depicted in Fig.1. The values of z_1 and z_2 are 2.5 mm and 5.0 mm, respectively. The measurements are taken at three time points: t = 25 min, 50 min, and 75 min.

(3) Since there is no actual measurement data, the pore water pressure sensors are assumed very accurate. The measured values of the sensors $\bar{p}(\xi_i;t_j)$ are obtained by taking exact consolidation coefficient c_{v} =0.858 6 mm^2/min into the analytical solution Eq.（21） which is given in Eq.（24）.

(4) Convergence is achieved when the specified condition is satisfied:

$$\mathrm{tol}=\left\|\Delta\boldsymbol{\eta}^{(l)}\right\|=\sqrt{\Delta c_{\mathrm{v}}^{(l)2}}<\varepsilon=1\times10^{-9} \tag{25}$$

where tol is the error value for computation; ε is the permissible error.

The numerical results of identifying the consolidation coefficient c_{v} using Gauss-Newton, Levenberg, Marquardt, Nielsen methods are shown in Table 1.

Table 1 presents two methods for evaluating identification speed: algorithm runtime and iteration count. Due to the inherent variability of runtime across different executions, this study adopts iteration count as a more consistent measure. This approach enables an investigation into the relationship between the damping coefficient and the number of iterations.

As shown in Table 1, when the damping parameter μ is less than 100, both the Gauss-Newton, Levenberg, Nielsen methods converge to the same solution c_{v} =0.858 6 mm^2/min after 6 iterations, however, when the

damping parameter μ is set to 100, the Marquardt method requires 1 071 iterations to reach the converged solution. On the other hand, when the damping parameter μ is set to 10 000, the Levenberg method requires 7 iterations and Nielsen methods requires 6 iterations, thus Nielsen method slightly speeds up convergence.

Table 1 Identification of c_v according to sensors arrangement and initial iteration value $c_v^{(1)}$=0.1

Method	μ	l/ iteration	t/s	c_v
Levenberg method	10^{-9}	6	0.008 1	0.858 6
	10^{-7}	6	0.007 2	0.858 6
	10^{-5}	6	0.006 3	0.858 6
	10^{-3}	6	0.006 3	0.858 6
	10^{-1}	6	0.006 8	0.858 6
	10^{0}	6	0.011 0	0.858 6
	10^{1}	6	0.007 1	0.858 6
	10^{2}	6	0.015 3	0.858 6
	10^{4}	7	0.022 3	0.858 6
Marquardt method	10^{-9}	6	0.014 8	0.858 6
	10^{-7}	6	0.011 1	0.858 6
	10^{-5}	6	0.007 2	0.858 6
	10^{-3}	6	0.008 1	0.858 6
	10^{-1}	8	0.007 0	0.858 6
	10^{0}	18	0.012 2	0.858 6
	10^{1}	114	0.022 6	0.858 6
	10^{2}	107 1	0.109 7	0.858 6
	10^{3}	106 40	0.873 3	0.858 6
Nielsen method	10^{-9}	6	0.011 9	0.858 6
	10^{-7}	6	0.011 4	0.858 6
	10^{-5}	6	0.014 9	0.858 6
	10^{-3}	6	0.015 3	0.858 6
	10^{-1}	6	0.025 7	0.858 6
	10^{0}	6	0.014 7	0.858 6
	10^{1}	6	0.023 7	0.858 6
	10^{2}	6	0.012 0	0.858 6
	10^{4}	6	0.010 3	0.858 6
Gauss-Newton method	0	6	0.007 1	0.858 6

To evaluate the robustness of algorithms, random noise was added to the measured pore water pressure:

$$p_N(z_i;t_j)=p(z_i;t_j)+\boldsymbol{N} \tag{26}$$

where the pore water pressure $p(z_i;t_j)$ is determined by Eq. (24); and the noise N is a random matrix with a normal distribution. Six random tests were conducted using the Gauss-Newton, Levenberg, Marquardt, and Nielsen methods, with a damping parameter $\mu=10^{-9}$. The average value of the consolidation coefficient from these six tests was then calculated. The average value $\bar{c}_v$ is compared with the correct consolidation coefficient c_v =0.858 6 mm^2/min, and the results are listed in Table 2. The error and the average number of iterations $\bar{l}$ was determined by the following equations:

$$\left.\begin{aligned}&\bar{c}_v=(c_{v1}+\cdots+c_{v6})/6\\&\mathrm{err}=\left|\bar{c}_v-0.858\,6\right|/0.858\,6\\&\bar{l}=(l_1+\cdots+l_6)/6\end{aligned}\right\} \tag{27}$$

As shown in Table 2, the error between the average value $\bar{c}_v$ and the correct value is at most 0.35%. This indicates that the Gauss-Newton, Levenberg, Marquardt, and Nielsen methods are highly effective for identifying the consolidation coefficient. When noise is applied, the algorithms demonstrates a certain level of robustness against it.

Table 2 Identification of c_v after adding noise

Methods	$\bar{c}_v$	err/%	$\bar{l}$
Gauss-Newton method	0.857 9	0.08	8.7
Levenberg method ($\mu=10^{-9}$)	0.855 6	0.35	8.7
Marquardt method ($\mu=10^{-9}$)	0.857 3	0.15	8.8
Nielsen method ($\mu=10^{-9}$)	0.860 3	0.20	8.8

4.2 Identification of the point source within a fluid-saturated poroelastic medium

This section focuses on the inverse problem of determining the coordinates of the point source in the Barry and Mercer consolidation model. The Gauss-Newton, Levenberg, Marquardt and Nielsen methods are employed, using the analytical solutions proposed by Barry et al.[28].

The dimensionless 2D Biot's consolidation theory for the point source problem can be written as [28]

$$\left.\begin{aligned}&(m+1)\frac{\partial^2 u}{\partial x^2}+\frac{\partial^2 u}{\partial z^2}+m\frac{\partial^2 w}{\partial x\partial z}=(m+1)\frac{\partial p}{\partial x}\\&\frac{\partial^2 w}{\partial x^2}+(m+1)\frac{\partial^2 w}{\partial z^2}+m\frac{\partial^2 u}{\partial x\partial z}=(m+1)\frac{\partial p}{\partial z}\\&\frac{\partial^2 p}{\partial x^2}+\frac{\partial^2 p}{\partial z^2}=\frac{\partial \phi}{\partial t}-\alpha Q\\&\phi=\frac{\partial u}{\partial x}+\frac{\partial w}{\partial z}\end{aligned}\right\} \tag{28}$$

where u,w represent the x,z components of solid displacements, respectively; p is a scaled applied pressure; m is an elastic parameter; α is a scaled source strength[28]; Q is the point source function (see eq.(29)), and ϕ is a scalar function.

The studied region is a rectangle of $0\leqslant x\leqslant a$ and $0\leqslant z\leqslant b$ as Fig. 2 shows, and the point source can be located at (x_0, z_0) and the imposed flow rate is

$$Q(x,y,t)=\delta\left(x-x_0\right)\delta\left(z-z_0\right)\sin\omega t \tag{29}$$

where δ is the Dirac delta function, and ω is angular frequency.

The boundary conditions of the displacement and pore pressure fields are

$$\left.\begin{aligned}&z=0:w=0,\frac{\partial u}{\partial x}=0,\ p=p_3(x,t)\\&z=b:w=0,\frac{\partial u}{\partial x}=0,\ p=p_4(x,t)\end{aligned}\right\} \tag{30}$$

$$\left.\begin{aligned}&x=0:u=0,\frac{\partial w}{\partial z}=0,\ p=p_1(x,t)\\&x=a:u=0,\frac{\partial w}{\partial z}=0,\ p=p_2(x,t)\end{aligned}\right\} \tag{31}$$

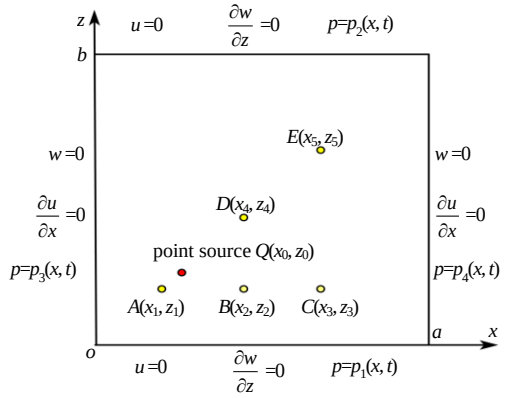


Fig.2 Layout of pore water pressure sensors within a rectangular poroelastic medium of dimensionless lengths *a*=1.0 and *b*=1.0.

The case of a point source at (x_0, z_0) and with zero pressure on the boundary such that $p_1 = p_2 = p_3 = p_4 = 0$ leads to the analytical solution[28]:

$$p(x,z,t) = -\frac{4}{ab}\sum_{q=1}^{\infty}\sum_{n=1}^{\infty}\frac{\alpha \sin\lambda_n x_0 \sin\lambda_q z_0}{\hat{\lambda}^2+\omega^2}\times \left(\hat{\lambda}\sin\omega t - \omega\cos\omega t + \omega e^{-\hat{\lambda}t}\right)\sin\lambda_n x \sin\lambda_q z \tag{32}$$

where $\hat{\lambda} = \lambda_n^2 + \lambda_q^2$; $\lambda_n = n\pi/a$; $\lambda_q = q\pi/b$; and n, q are positive integers.

The following work is finding exact point source coordinates $Q(0.25, 0.25)$ based on Barry-Mercer analytical solution (Eq.(32)) and pore water pressure measured values of sensors at $A(x_1, z_1)$, $B(x_2, z_2)$, $C(x_3, z_3)$ or $A(x_1,z_1)$, $D(x_4, z_4)$, $E(x_5, z_5)$.

According to the Eqs.（7） and （8）, the Jacobian matrix $\boldsymbol{A}$ and the l(th) iteration pore water pressure $p(\boldsymbol{\eta}^{(l)};\xi_i;t_j)$ are

$$\frac{\partial p(\boldsymbol{\eta}^{(l)};\xi_i;t_j)}{\partial x_0} = -\frac{4}{ab}\sum_{q=1}^{\infty}\sum_{n=1}^{\infty}\frac{\alpha\lambda_n \cos\lambda_n x_0^{(l)} \sin\lambda_q z_0^{(l)}}{\hat{\lambda}^2+\omega^2}\times \left(\hat{\lambda}\sin\omega t_j - \omega\cos\omega t_j + \omega e^{-\hat{\lambda}t_j}\right)\sin\lambda_n x_i \sin\lambda_q z_i \tag{33}$$

$$\frac{\partial p(\boldsymbol{\eta}^{(l)};\xi_i;t_j)}{\partial z_0} = -\frac{4}{ab}\sum_{q=1}^{\infty}\sum_{n=1}^{\infty}\frac{\alpha\lambda_q \sin\lambda_n x_0^{(l)} \cos\lambda_q z_0^{(l)}}{\hat{\lambda}^2+\omega^2}\times \left(\hat{\lambda}\sin\omega t_j - \omega\cos\omega t_j + \omega e^{-\hat{\lambda}t_j}\right)\sin\lambda_n x_i \sin\lambda_q z_i \tag{34}$$

$$p(\boldsymbol{\eta}^{(l)};\xi_i;t_j) = -\frac{4}{ab}\sum_{q=1}^{\infty}\sum_{n=1}^{\infty}\frac{\alpha \sin\lambda_n x_0^{(l)} \sin\lambda_q z_0^{(l)}}{\hat{\lambda}^2+\omega^2}\times \left(\hat{\lambda}\sin\omega t_j - \omega\cos\omega t_j + \omega e^{-\hat{\lambda}t_j}\right)\sin\lambda_n x_i \sin\lambda_q z_i \tag{35}$$

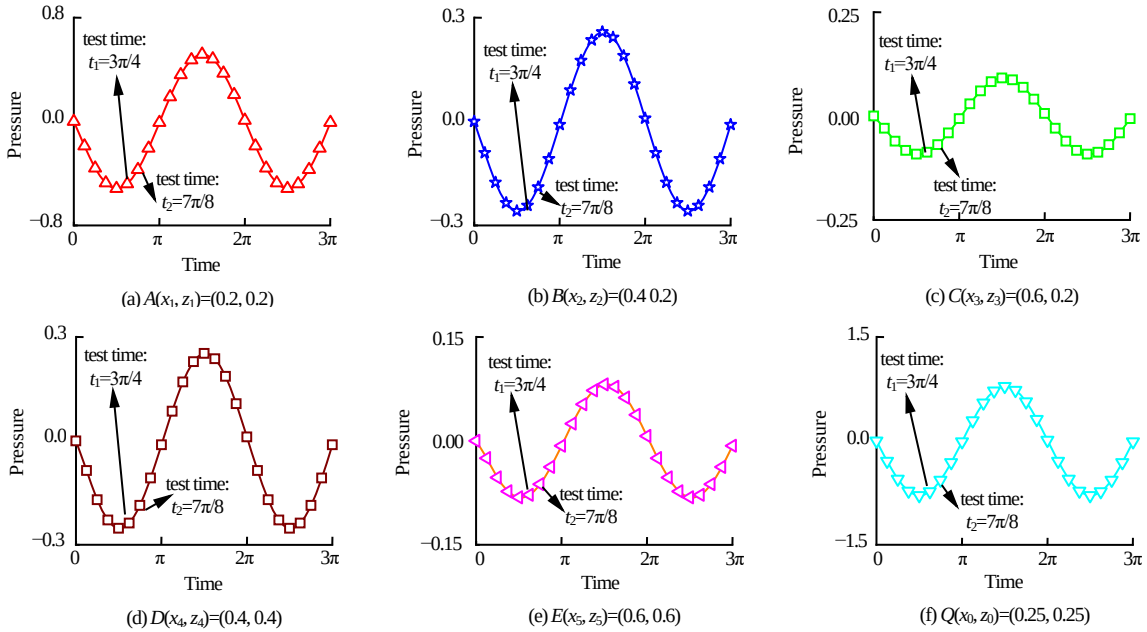


Fig.3 Pore water pressure time history curves at different location of sensors

where vector $\boldsymbol{\eta}^{(l)}$ represents the set of l(th) iteration parameters that need to be identified, $\boldsymbol{\eta}^{(l)} = [x_0^{(l)}, z_0^{(l)}]$; and ξ_i is the sensor location's coordinate, $\xi_i = (x_i, z_i)$.

Assuming that the pore water pressure sensor is very accurate, the results of the measurement $\bar{p}(\xi_i;t_j)$ is the analytical solutions (Eq.（32）) of the pore water pressure generated by the location point source Q(0.25, 0.25) as Fig. 2 shows:

$$\bar{p}(\xi_i;t_j) = -\frac{4}{ab}\sum_{q=1}^{\infty}\sum_{n=1}^{\infty}\frac{\alpha \sin\lambda_n x_0 \sin\lambda_q z_0}{\hat{\lambda}^2+\omega^2}\times \left(\hat{\lambda}\sin\omega t_j - \omega\cos\omega t_j + \omega e^{-\hat{\lambda}t_j}\right)\sin\lambda_n x_i \sin\lambda_q z_i \tag{36}$$

The parameter values of the analytical solution Eq.（32） are specified in accordance with the literature by Barry et al[28]:

(1) The location of the point source is Q(0.25, 0.25), which is used to calculate three sensor measurements and to

verify the validity of the proposed methods.

(2) Here are two ways to arrange the pore water pressure sensors:

i) $A(x_1, z_1)$=(0.2, 0.2), $B(x_2, z_2)$=(0.4, 0.2), $C(x_3, z_3)$= (0.6, 0.2）; ii) $A(x_1, z_1)$=(0.2, 0.2), $D(x_4, z_4)$=(0.4, 0.4), $E(x_5, z_5)$=(0.6, 0.6).

Since there is no actual measurement data, the sensors are assumed very accurate and the measured values of the sensors are obtained by taking (x_i, y_i) ($i=1,2,3$ or $i=1,4,5$) and $Q(x_0, y_0)=(0.25, 0.25)$ into the analytical solution Eq.（36）.

(3) The initial iteration coordinates of the point source are ($x_0^{(1)}$, $z_0^{(1)}$)=(0.05, 0.05) and ($x_0^{(1)}$, $z_0^{(1)}$)=(0.01, 0.01).

(4) The pore water pressure needs to be chosen at the right time so that the pore water pressure function $\bar{p}(\xi_i; t_j)$ is monotonic. This will make sure that the correct solution for convergence is found. As shown in Fig.3, the pore pressure function $\bar{p}(\xi_i; t_j)$ is monotonically increasing in the time interval, so t_1 =3π/4 and t_2 =7π/8 are chosen for the Gauss-Newton, Levenberg, Marquardt and Nielsen methods.

(5) Other parameter values are the same as in the literature by Barry and Mercer[28]:

(6) Convergence occurs when the following condition is met:

$$\text{tol}=\sqrt{\Delta x_0^{(l)2}+\Delta z_0^{(l)2}}<\varepsilon=1\times10^{-9} \quad (37)$$

Otherwise, iterations terminate when the iteration count exceeds a pre-specified limit and the iteration count is 1 000.

The details of the Gauss-Newton, Levenberg, Marquardt, and Nielsen methods can be seen in Figs. 4 and 5. Tables 3–6 show the numerical results of algorithms.

As shown in Tables 3-6, the Gauss-Newton method converges to (27.75, −14.25), (395.7364, −406.1819), (241.75, 117.75) and (2.25, −3.75), so the Gauss-Newton cannot converge to the correct point source Q(0.25, 0.25), but the Levenberg, Marquardt, and Nielsen methods may converge to the correct point source Q(0.25, 0.25).

Table 3 shows when the damping parameter $\mu=20$, the Levenberg, Marquardt and Nielsen methods reach the same convergent solution (0.263 6, 0.181 9) after 223, 939 and 12 iteration steps respectively at sensors arrangement (A, B, C) and initial iteration point $(x_0^{(1)}, z_0^{(1)})=(0.05, 0.05)$. It is clear that the Nielsen method speeds up convergence. On the other hand, compared to the Levenberg method, the Marquardt method extends the valid range of damping parameter from [0.05, 1.00] to [0.25, 2.25] (1.00−0.05=0.95 to 2.25−0.25=2.00) but reduces the speed of convergence.

Tables 4 and 6 represent that valid intervals of the damping parameter μ are [0.25, 0.75]∪[1.50, 2.75]∪[9.00, 10.25] and [0.25]∪[1.00, 5.25]∪[7.50, 10.25] by the Nielsen method in which the coordinates converge to the correct point source Q(0.25, 0.25), thus the Nielsen method may result in discontinuous valid intervals for the damping parameter and more convergence point sources, which increases the difficulty of accurately determining the point source.

Algorithm 1: Pseudocode for Gauss-Newton, Levenberg and Marquardt methods

```
Input: Coordinates of sensors (A, B, C or A, D, E)
Input: α = 2.0 , a=b=1.0, ω = 2.0
Input: test time: t = [3π / 4, 7π / 8]
initial iteration: η^(1) = (x_0^(1), z_0^(1))
/* (x_0^(1), z_0^(1)) = (0.01, 0.01) or (0.05, 0.05) */
Output: the location of point source
ε = 1×10^−9 and ‖Δη^(1)‖ = 1.0
iteration number: count =1
while ‖Δη^(l)‖ > ε do
for i ← 1 to 3(three sensors positions) do
  for j ← 1 to 2(two test time data) do
    for n ← 1 to 10 do
      for q ← 1 to 10 do
          Eq.（36）(sensors measurements)
          Eq.（35）(iteration values)
        end
    end
  end
end
compute error vector: Eq.（8）
compute Jacobian matrix Eq.（7）
damping parameter μ
Gauss-Newton method: Δη^(l) [Eq.（6）]
Levenberg method: Δη^(l) [(Eq.（15）]
Marquardt method: Δη^(l) [Eq.（17）]
update the point source η^(l+1) = η^(l) + Δη^(l)
compute tolerance ‖Δη^(l)‖
iteration number: count=count+1
If η^(l+1) =(0.25, 0.25) then
   break
end
If count>1 000 then
   break
end
 end
```

Fig.4 Pseudocode for Gauss-Newton, Levenberg and Marquardt methods

Table 5 demonstrates the point source will converge to the correct solution Q (0.25, 0.25) using the Levenberg, Marquardt, and Nielsen methods only if the damping parameter μ is set to any value in this interval [1×10^{-7}, 1.00]. Therefore, the exact point source can be determined using a smaller positive damping parameter whose valid intervals are close to half-open interval (0, a] (a is a number greater than or equal to 1.00), which is easier to select than choosing a number from a specific interval in the positive real number domain as required in Tables 3, 4, and 6. Therefore, the sensor arrangement (A, D, E) and the initial

iteration point source (0.05, 0.05) are deemed the most suitable sensor configuration and initial iteration point.

Algorithm 2: Pseudocode for Nielsen method

Input: Coordinates of sensors(*A*, *B*, *C* or *A*, *D*, *E*)
Input: $\alpha = 2.0$, a =*b*=1.0, $\omega = 2.0$
Input: test time: $t = [3\pi / 4, 7\pi / 8]$
initial iteration: $\boldsymbol{\eta}^{(1)} = (x_0^{(1)}, z_0^{(1)})$
/* $(x_0^{(1)}, z_0^{(1)}) = (0.01, 0.01)$ or $(0.05, 0.05)$ */
Output: the location of point source
$\varepsilon = 1\times10^{-9}$ and $\| \Delta\boldsymbol{\eta}^{(1)}\| = 1.0$
iteration number: count =1
damping parameter μ
while $\| \Delta\boldsymbol{\eta}^{(l)}\| > \varepsilon$
for $i \leftarrow$ 1 to 3(three sensors positions) do
  for $j \leftarrow$ 1 to 2(two test time data) do
    for $n \leftarrow$ 1 to 10 do
      for $q \leftarrow$ 1 to 10 do
        Eq.（36）(sensors measurements)
        Eq.（35）(iteration values)
      end
    end
  end
end
compute error vector: Eq.（8）
compute least squares function Eq.（1）
compute Jacobian matrix Eq.（7）
Nielsen method: $\Delta\boldsymbol{\eta}^{(l)}$ [(Eq.（15）]
update the point source $\boldsymbol{\eta}^{(l+1)} = \boldsymbol{\eta}^{(l)} + \Delta\boldsymbol{\eta}^{(l)}$
compute tolerance $\| \Delta\boldsymbol{\eta}^{(l)}\|$
iteration number: count=count+1
update least squares function Eq.（1）
compute the gain ratio ρ （Eq.（19））
If $\rho > 0$ then
  $\mu = \mu \times \max\{1/3, 1-(2\rho-1)^3\}; \nu = 2$
else
  $\mu = \mu \times \nu; \nu = 2\times\nu$
end
If $\eta^{(l+1)} = (0.25, 0.25)$ then
  break
end
end

Fig.5 Pseudocode for Nielsen method

Tables 3–6 indicate how the valid intervals of the damping parameter vary significantly with the sensors location and initial iteration point source for various algorithms. For instance, when considering the arrangement of sensors (*A*, *D*, *E*) and the initial iteration point source (0.05, 0.05) as presented in Table 5, the Levenberg method determines the valid interval for the damping parameter is $[1\times10^{-7}, 1.25]$. This interval is considered plausible. However, when the initial iteration point source is changed to (0.01, 0.01) as shown in Table 6, only two values of the damping parameter (0.25 and 1.25) are able to accurately identify the source point using the Levenberg method. Therefore, it is crucial to select appropriate initial iterative points. When the damping parameter exceeds a threshold, the Levenberg and Marquardt methods converge the point source to a single value, whereas the Nielsen method permits the point source to converge to multiple values. For example, as shown in Table 5, when the damping parameter $\mu \geqslant 2.5$, the point source converges to the coordinates (0.161 8, 0.161 8) using the Marquardt and

Table 3 Point source identification according to sensors arrangement (*A*, *B*, *C*) and initial iteration source (0.05, 0.05)

Methods	μ	l	x_0	z_0	Note
Levenberg method	0.001	136	−6.263 6	−16.181 9	$\mu \in [0.05, 1.00]$ *
	0.010	9	−0.250 0	−0.250 0	
	0.050	6	0.250 0	0.250 0	
	0.250	7	0.250 0	0.250 0	
	0.500	6	0.250 0	0.250 0	
	0.750	10	0.250 0	0.250 0	
	1.000	16	0.250 0	0.250 0	
	1.250	21	0.263 6	0.181 9	
	1.500	26	0.263 6	0.181 9	
	2.000	23	0.263 6	0.181 9	
	2.250	31	0.263 6	0.181 9	
	2.500	33	0.263 6	0.181 9	
	5.000	60	0.263 6	0.181 9	
	20.000	223	0.263 6	0.181 9	
Marquardt method	0.001	37	371.736 4	−24.181 9	$\mu \in [0.25, 2.25]$ *
	0.010	26	9.736 4	−18.181 9	
	0.050	8	0.263 6	0.181 9	
	0.250	17	0.250 0	0.250 0	
	0.500	24	0.250 0	0.250 0	
	0.750	26	0.250 0	0.250 0	
	1.000	32	0.250 0	0.250 0	
	1.250	15	0.250 0	0.250 0	
	1.500	35	0.250 0	0.250 0	
	2.000	64	0.250 0	0.250 0	
	2.250	61	0.250 0	0.250 0	
	2.500	209	0.263 6	0.181 9	
	5.000	455	0.263 6	0.181 9	
	20.000	939	0.263 6	0.181 9	
Nielsen method	0.001	7	1.750 0	−4.250 0	$\mu \in [0.01, 0.75]$ *
	0.010	17	0.250 0	0.250 0	
	0.050	4	0.250 0	0.250 0	
	0.250	6	0.250 0	0.250 0	
	0.500	4	0.250 0	0.250 0	
	0.750	6	0.250 0	0.250 0	
	1.000	7	0.263 6	0.181 9	
	1.250	10	0.263 6	0.181 9	
	1.500	11	0.263 6	0.181 9	
	2.000	9	0.263 6	0.181 9	
	2.250	9	0.263 6	0.181 9	
	2.500	9	0.263 6	0.181 9	
	5.000	10	0.263 6	0.181 9	
	20.000	12	0.263 6	0.181 9	
Gauss-Newton method	0.000	28	27.750 0	−14.250 0	—

Note: * The point source converges to the correct solution Q(0.25, 0.25) when damping parameter μ takes a value in the interval. The sensors are arranged at $A(x_1, z_1)$=(0.2, 0.2), $B(x_2, z_2)$=(0.4, 0.2), $C(x_3, z_3)$=(0.6, 0.2).

Levenberg method. However, the Nielsen method converges multiple point sources, which include (3.75, −4.25), (−0.25, −0.25), and (4.25, 2.25). More convergent values make it more difficult to identify the correct point source Q(0.25, 0.25).

Table 4 Point source identification according to sensors arrangement (*A*, *B*, *C*) and initial iteration source (0.01, 0.01)

Methods	μ	l	x_0	z_0	Notes
Levenberg method	0.001	12	1.750 0	1.750 0	$\mu\in[0.05,0.50]$ *
	0.010	9	1.750 0	1.750 0	
	0.050	11	0.250 0	0.250 0	
	0.250	9	0.250 0	0.250 0	
	0.500	18	0.250 0	0.250 0	
	0.750	15	0.181 9	0.181 9	
	1.000	17	0.181 9	0.181 9	
	1.250	17	0.181 9	0.181 9	
	1.500	21	0.181 9	0.181 9	
	2.000	30	0.181 9	0.181 9	
	2.250	32	0.181 9	0.181 9	
	2.500	34	0.181 9	0.181 9	
	5.000	61	0.181 9	0.181 9	
	10.000	116	0.181 9	0.181 9	
	20.000	227	0.181 9	0.181 9	
Marquardt method	0.001	25	−84.263 6	17.818 1	$\mu\in[1.25,9.50]$ *
	0.010	46	−1.750 0	10.250 0	
	0.050	29	12.250 0	−1.750 0	
	0.250	15	−11.736 4	−3.818 1	
	0.500	17	−0.263 6	−0.181 9	
	1.000	61	−4.250 0	−2.250 0	
	1.250	57	0.250 0	0.250 0	
	2.000	67	0.250 0	0.250 0	
	3.000	125	0.250 0	0.250 0	
	5.000	185	0.250 0	0.250 0	
	7.000	193	0.250 0	0.250 0	
	9.500	248	0.250 0	0.250 0	
	9.750	248	0.263 6	0.181 9	
	10.000	553	0.263 6	0.181 9	
	20.000	868	0.263 6	0.181 9	
Nielsen method	0.001	21	−1.736 4	4.181 9	$\mu\in[0.25,0.75]\cup$ [1.50, 2.75]$\cup$ [9.00,10.25]*
	0.010	15	1.750 0	−0.250 0	
	0.050	17	0.263 6	0.181 9	
	0.250	8	0.250 0	0.250 0	
	0.750	14	0.250 0	0.250 0	
	1.000	10	0.263 6	0.181 9	
	1.250	9	0.263 6	0.181 9	
	1.500	7	0.250 0	0.250 0	
	2.750	8	0.250 0	0.250 0	
	3.000	6	0.263 6	0.181 9	
	8.750	10	0.263 6	0.181 9	
	9.000	9	0.250 0	0.250 0	
	10.250	9	0.250 0	0.250 0	
	10.500	10	0.263 6	0.181 9	
	20.000	11	0.263 6	0.181 9	
Gauss-Newton method	0.000	17	395.736 4	−406.181 9	—

Note: * The point source converges to the correct solution Q(0.25, 0.25) when damping parameter μ takes a value in the interval. The sensors are arranged at $A(x_1, z_1)$=(0.2, 0.2), $B(x_2, z_2)$=(0.4, 0.2), $C(x_3, z_3)$=(0.6, 0.2).

Table 5 Point source identification according to sensors arrangement (*A*, *D*, *E*) and initial iteration source (0.05, 0.05)

Methods	μ	l	x_0	z_0	Notes
Levenberg method	1×10^{-8}	72	79.750 0	−130.250 0	$\mu\in[1\times10^{-7},1.00]$ *
	1×10^{-7}	9	0.250 0	0.250 0	
	1×10^{-4}	4	0.250 0	0.250 0	
	0.001	4	0.250 0	0.250 0	
	0.010	5	0.250 0	0.250 0	
	0.050	5	0.250 0	0.250 0	
	1.000	4	0.250 0	0.250 0	
	1.250	6	0.250 0	0.250 0	
	2.000	6	0.161 8	0.161 8	
	2.250	7	0.161 8	0.161 8	
	2.500	7	0.161 8	0.161 8	
	5.000	9	0.161 8	0.161 8	
	10.000	13	0.161 8	0.161 8	
Marquardt method	1×10^{-9}	19	−36.250 0	23.750 0	$\mu\in[1\times10^{-8},2.25]$ *
	1×10^{-8}	13	0.250 0	0.250 0	
	1×10^{-4}	4	0.250 0	0.250 0	
	0.001	4	0.250 0	0.250 0	
	0.010	5	0.250 0	0.250 0	
	0.050	5	0.250 0	0.250 0	
	0.500	7	0.250 0	0.250 0	
	1.500	9	0.250 0	0.250 0	
	2.000	11	0.250 0	0.250 0	
	2.250	13	0.250 0	0.250 0	
	2.500	15	0.161 8	0.161 8	
	5.000	25	0.161 8	0.161 8	
	10.000	48	0.161 8	0.161 8	
Nielsen method	1×10^{-9}	39	−6.250 0	23.750 0	$\mu\in[1\times10^{-8},1.25]\cup$ [2.50, 2.51]*
	1×10^{-8}	12	0.250 0	0.250 0	
	1×10^{-4}	4	0.250 0	0.250 0	
	0.001	4	0.250 0	0.250 0	
	0.010	4	0.250 0	0.250 0	
	0.500	4	0.250 0	0.250 0	
	1.250	51	0.250 0	0.250 0	
	1.500	42	0.250 0	4.250 0	
	2.500	28	0.250 0	0.250 0	
	2.510	28	0.250 0	0.250 0	
	2.520	28	3.750 0	−4.250 0	
	5.000	37	−0.250 0	−0.250 0	
	10.000	33	4.250 0	2.250 0	
Gauss-Newton method	0.000	60	241.750 0	117.750 0	—

Note: * The point source converges to the correct solution Q(0.25, 0.25) when damping parameter μ takes a value in the interval. The sensors are arranged at $A(x_1, z_1)$=(0.2, 0.2), $D(x_4, z_4)$=(0.4, 0.4), $E(x_5, z_5)$=(0.6, 0.6).

On the other hand, the range of effective damping parameter Marquardt method is superior to the Nielsen and Levenberg for identifying the point source.

To assess the robustness of the algorithms, random noise was introduced into the measured pore water pressure:

$$p_N(\boldsymbol{\eta}_i;t_j)=p(\boldsymbol{\eta}_i;t_j)+\boldsymbol{N} \quad (38)$$

As indicated in Table 5, with a damping parameter of $\mu=1\times10^{-4}$, both the Levenberg, Marquardt and Nielsen methods successfully converge to the accurate solution of (0.25, 0.25). Six random tests were performed using the Levenberg, Marquardt, and Nielsen methods, with a

Table 6 Point source identification according to sensors arrangement (*A*, *D*, *E*) and initial iteration source (0.01, 0.01)

Methods	μ	l	x_0	z_0	Notes
Levenberg method	0.001	224	27.750 0	9.750 0	$\mu \in [0.25] \cup [1.25]$ *
	0.010	253	1.749 9	3.750 1	
	0.050	5	0.783 1	0.783 1	
	0.250	4	0.250 0	0.250 0	
	0.500	4	0.161 8	0.161 8	
	0.750	5	0.161 8	0.161 8	
	1.000	7	0.161 8	0.161 8	
	1.250	8	0.250 0	0.250 0	
	1.500	7	0.161 8	0.161 8	
	2.000	7	0.161 8	0.161 8	
	2.250	8	0.161 8	0.161 8	
	2.500	8	0.161 8	0.161 8	
	5.000	10	0.161 8	0.161 8	
	10.000	15	0.161 8	0.161 8	
	20.000	25	0.161 8	0.161 8	
Marquardt method	0.50	8	0.783 1	0.783 1	$\mu \in [4.00, 10.00]$ *
	0.75	4	0.783 1	0.783 1	
	1.00	9	0.783 1	0.783 1	
	1.25	11	0.783 1	0.783 1	
	1.50	11	0.783 1	0.783 1	
	2.00	6	0.485 6	0.485 6	
	3.00	7	0.485 6	0.485 6	
	3.50	9	0.485 6	0.485 6	
	4.00	22	0.250 0	0.250 0	
	5.00	25	0.250 0	0.250 0	
	10.00	40	0.250 0	0.250 0	
	10.25	40	0.161 8	0.161 8	
	12.50	28	0.161 8	0.161 8	
	15.00	61	0.161 8	0.161 8	
	20.00	91	0.161 8	0.161 8	
Nielsen method	0.10	52	−0.250 0	−0.250 0	$\mu \in [0.25] \cup [1.00, 5.25] \cup [7.50, 10.75]$*
	0.25	4	0.250 0	0.250 0	
	0.50	40	1.750 0	−0.250 0	
	0.75	21	−1.750 0	2.250 0	
	1.00	9	0.250 0	0.250 0	
	5.25	21	0.250 0	0.250 0	
	5.50	38	−1.169 3	−1.296 4	
	7.00	42	−0.250 0	−0.250 0	
	7.25	39	−2.250 0	−0.250 0	
	7.50	8	0.250 0	0.250 0	
	10.75	8	0.250 0	0.250 0	
	11.00	50	9.750 0	5.750 0	
	11.25	68	−1.750 0	14.250 0	
	15.00	65	15.750 0	15.750 0	
	20.00	37	−2.250 0	9.750 0	
Gauss-Newton method	0.00	15	2.250 0	−3.750 0	—

Note: * The point source converges to the correct solution Q (0.25, 0.25) when damping parameter μ takes a value in the interval. The sensors are arranged at $A(x_1, z_1)$=(0.2, 0.2), $D(x_4, z_4)$=(0.4, 0.4), $E(x_5, z_5)$=(0.6, 0.6).

damping parameter $\mu = 1 \times 10^{-4}$ and the sensor arrangement (*A*, *D*, *E*) and the initial iteration point source (0.05, 0.05). The accuracy of identification depends on the level of noise applied. When the noise is relatively small compared to the precise measurements, the identification is more effective. However, when the noise is significant, it becomes difficult to accurately identify the point source (0.25, 0.25). In this study, a small amount of noise was applied and the identification results, as shown in Table 7, demonstrate minimal error from the exact point source (0.25, 0.25). Thus, the Levenberg, Marquardt, and Nielsen methods exhibit robustness against noise.

Table 7 Identification of (x_0, z_0) after adding noise

Methods	(x_0, z_0)	l
Levenberg method	(0.250 0, 0.250 0)	4
	(0.250 0, 0.250 0)	4
	(0.250 0, 0.250 0)	4
	(0.241 7, 0.257 1)	12
	(0.243 9, 0.255 4)	13
	(0.250 0, 0.250 0)	4
Marquardt method	(0.253 7, 0.246 5)	14
	(0.255 4, 0.243 8)	14
	(0.254 0, 0.245 3)	13
	(0.250 0, 0.250 0)	4
	(0.253 3, 0.246 4)	14
	(0.252 8, 0.246 6)	12
Nielsen method	(0.250 0, 0.250 0)	4
	(0.250 0, 0.250 0)	4
	(0.250 0, 0.250 0)	4
	(0.241 7, 0.257 1)	12
	(0.243 9, 0.255 4)	12
	(0.249 9, 0.249 9)	33

Note: Damping parameter $\mu = 0.0001$ and the sensor arrangement is (*A*, *D*, *E*). The initial iteration point source is (0.05, 0.05).

5 Discussions

The theory of consolidation is fundamental to soil mechanics. Traditional studies typically involve solving the consolidation differential equation to obtain an analytical solution for pore water pressure. This paper explores an inverse problem in consolidation theory, focusing on extracting relevant geotechnical parameters from pore water pressure measurements and corresponding analytical solutions. However, geotechnical engineering encompasses various variables that vary temporally and spatially, including stress, strain, displacement, and pore water pressure. This study separates time and spatial variables in the pore water pressure function, resulting in the development of a novel Jacobian matrix that accommodates any number of time points and spatial coordinates. The update rules for the Gauss-Newton, Levenberg, Marquardt, and Nielsen methods are then derived.

The effectiveness of the proposed algorithm is validated through two numerical examples. Case 1 involves identifying the consolidation coefficient in Terzaghi's classical consolidation model, using 2 coordinate variables and 3 time points. Case 2 aims to identify the point source in the analytical solution of Barry and Mercer problem within a saturated porous medium, based on poroelastic consolidation equations, using 3 coordinate variables and 2 time points. The results clearly demonstrate the algorithm's capability in identifying model parameters. Compared to the

PINNs for geotechnical parameter identification, the proposed method offers the advantage of requiring fewer measurements and shorter time, thus enabling the identification of relevant geotechnical parameters in consolidation models more efficiently.

It should be noted that the identification of the Terzaghi classical consolidation model assumes a constant consolidation coefficient with respect to pore water pressure. However, in some measurements, the consolidation coefficient can change significantly as the pore water pressure dissipates, indicating that soil consolidation is a nonlinear process[35−37]. Therefore, the algorithm has limitations when identifying consolidation coefficients; it is only applicable for short measurement intervals where the consolidation coefficient can be assumed constant. In such cases, the identified consolidation coefficient reflects the consolidation behavior over that short period. To address the issue of nonlinear consolidation coefficient identification, a nonlinear consolidation model could be adopted, with an analytical solution for pore water pressure variation over time to further verify the algorithm's accuracy.

In recent years, the use of PINNs to predict consolidation model parameters has gained widespread attention. However, many challenges remain unresolved in the theoretical and practical applications of PINNs. One major obstacle to using PINNs for solving PDEs is the excessively long training time, which stems from the use of first-order gradient methods. A promising solution is to employ faster second-order optimization algorithms for training neural networks to solve PDEs. The Levenberg-Marquardt algorithm is a well-known second-order gradient optimization method[38]. A key factor in the Levenberg-Marquardt method is how the gradient is defined, which involves the Jacobi matrix. The time- and space-varying Jacobi matrix (Eq.（7）) proposed in this paper could be an important aspect to investigate in its application to PINNs and it deserves further research in geotechnical engineering.

6 Conclusions

This paper presents four methods for identifying parameters related to the analytical solution of two consolidation models and pore water pressure measurements. Considering the temporal and spatial variations of pore water pressure, a novel Jacobi matrix accounting for both time and spatial variables in pore water pressure is constructed. The main conclusions can be drawn as follows:

(1) For the consolidation coefficient identification problem in 1D Terzaghi's consolidation model, all four methods (Gauss-Newton, Levenberg, Marquardt, and Nielsen methods) accurately identify the consolidation coefficient. A larger damping parameter leads to slower convergence with the Marquardt method.

(2) For the point source identification in Biot's 2D poroelastic problem, the Gauss-Newton method fails to determine the correct location of the point source. The Nielsen method accelerates convergence but results in discontinuous intervals for the effective damping coefficient, complicating the determination of the point source location. The Marquardt method slows convergence but expands the valid range of the damping parameter. The Marquardt method is better than the Levenberg and Nielsen methods. Suitable arrangement of pore water pressure sensors and the initial iteration location of the point source results in a plausible interval for the damping parameter.

(3) When random noise is introduced and the appropriate damping parameter is chosen, the results validate the robustness of the algorithms for parameter identification in both consolidation models.

Declaration of competing interest

The authors declare that they have no known competing financial interests or personal relationships that could have appeared to influence the work reported in this paper.

References

[1] KNAPPETT J A, CRAIG R F. Craig's soil mechanics[M]. 9th ed. New York: CRC Press, 2020: 115-117, 125−127.

[2] GIODA G, MAIER G. Direct search solution of an inverse problem in elastoplasticity: identification of cohesion, friction angle and in situ stress by pressure tunnel tests[J]. **International Journal for Numerical Methods in Engineering**, 1980, 15(12): 1823−1848.

[3] PAL S, WATHUGALA G, KUNDU S. Calibration of a constitutive model using genetic algorithms[J]. **Computers and Geotechnics**, 1996, 19(4): 325−348.

[4] SIMPSOM A, PRIEST S. The application of genetic algorithms to optimization problems in geotechnics[J]. **Computers and Geotechnics**, 1993, 15(1): 1−19.

[5] JIN Y, YIN Z, SHEN S, et al. Investigation into MOGA for identifying parameters of a critical-state-based sand model and parameters correlation by factor analysis[J]. **Acta Geotechnica**, 2016, 11(5): 1131−1145.

[6] YIN Z, JIN Y, SHEN J, et al. Optimization techniques for identifying soil parameters in geotechnical engineering: comparative study and enhancement[J]. **International Journal for Numerical and Analytical Methods in Geomechanics**, 2018, 42(1): 70−94.

[7] LEVENBERG K A. A method for the solution of certain non-linear problems in least squares[J]. **The Quarterly of Applied Mathematics**, 1944, 2(4): 164−168.

[8] MARQUARDT D W. An algorithm for least-squares estimation of non-linear parameters[J]. **Journal of the Society for Industrial and Applied Mathematics**, 1963, 11(2): 431−441.

[9] ZENTAR R, HICHER P, MOULIN G. Identification of soil parameters by inverse analysis[J]. **Computers and Geotechnics**, 2001, 28(2): 129−144.

[10] YIN Z, HICHER P. Identifying parameters controlling soil delayed behaviour from laboratory and in situ pressuremeter testing[J]. **International Journal for Numerical and Analytical Methods in Geomechanics**, 2008, 32(12): 1515−1535.

[11] FINNO R, CALVELLO M. Supported excavations: Observational method and inverse modeling[J]. **Journal of Geotechnical and Geoenvironmental Engineering**, 2005, 131(7): 826−836.

[12] LUCO J, WONG H. Identification of soil properties from foundation impedance functions[J]. **Journal of Geotechnical Engineering**, 1992, 118(5): 780−795.

[13] NAGARAJAIAH S, LI Z. Time segmented least squares identification of base isolated buildings[J]. **Soil Dynamics and Earthquake Engineering**, 2004, 24(8): 577−586.

[14] SAMUI P, KARTHIKEYAN J. Determination of liquefaction susceptibility of soil: a least square support vector machine approach[J]. **International Journal for Numerical and Analytical Methods in Geomechanics**, 2013, 37(9): 1154−1161.

[15] WU Xun, SHI Jian-yong, ZHANG Tao, et al. Inverse estimation of parameters for heat generation due to degradation in landfills based on the Levenberg-Marquardt algorithm[J]. **Rock and Soil Mechanics**, 2022, 43(2): 511−518.

[16] BAO Tai, LIU Xin-rong, ZHU Fan, et al. Least square method for the consolidation coefficient evaluation[J]. **Chinese Journal of Geotechnical Engineering**, 2005, 27(10): 1230−1232.

[17] XIAO Yan-li, LI Ming-xing. Overview of Levenberg-Marquardt algorithm[J]. **Software Guide**, 2018, 17(8): 9−12.

[18] RAISSI M, PERDIKARIS P, KARNIADAKIS G. Physics-informed neural networks: a deep learning framework for solving forward and inverse problems involving nonlinear partial differential equations[J]. **Journal of Computational Physics**, 2019, 378: 686−707.

[19] BEKELE Y. Physics-informed deep learning for one-dimensional consolidation[J]. **Journal of Rock Mechanics and Geotechnical Engineering**, 2021, 13(2): 420−430.

[20] AMINI D, HAGHIGHAT E, JUANES R. Inverse modeling of nonisothermal multiphase poromechanics using physics-informed neural networks[J]. **Journal of Computational Physics**, 2023, 490. DOI:10.1016/j.jcp.2023.112323.

[21] GONG W, ZUO L, LI L, et al. Prediction of stratified ground consolidation via a physics-informed neural network utilizing short-term excess pore water pressure monitoring data[J]. **Computer-Aided Civil and Infrastructure Engineering**, 2025, 40(2): 147−165.

[22] KARNIADAKIS G, KEVREKIDIS I, LU L, et al. Physics-informed machine learning[J]. **Nature Reviews Physics**, 2021, 3(6): 422−440.

[23] HUANG A B, LEE J T, HO Y T, et al. Stability monitoring of rainfall-induced deep landslides through pore pressure profile measurements[J]. **Soils and Foundations**, 2012, 52(4): 737−747.

[24] FENG W Q, LIU Z Y, TAM H Y, et al. The pore water pressure sensor based on Sagnac interferometer with polarization-maintaining photonic crystal fiber for the geotechnical engineering[J]. **Measurement**, 2016, 90: 208−214.

[25] ZHANG Yi-ping, YU Ya-nan, ZHANG Tu-qiao, et al. A method for evaluating coefficient of consolidation[J]. **Chinese Journal of Geotechnical Engineering**, 2002, 24(5): 616−618.

[26] BAO Tai, LIU Xin-rong. Consolidation coefficient evaluation using an improved genetic algorithm[J]. **Journal of Civil & Architectural & Environmental Engineering**, 2009, 31(1): 23−26.

[27] BIOT M. General theory of three-dimensional consolidation[J]. **Journal of Applied Physics**, 1941, 12(2): 155−164.

[28] BARRY S I, MERCER G N. Exact solutions for two dimensional time-dependent flow and deformation within a poroelastic medium[J]. **Journal of Applied Mechanics**, 1999, 66(2): 536−540.

[29] LI P C, LU D T. An analytical solution of two-dimensional flow and deformation coupling due to a point source within a finite poroelastic media[J]. **Journal of Applied Mechanics**, 2011, 78(6): 061020.

[30] LI P C, WANG K Y, LI X G, et al. Analytical solutions of a finite two-dimensional fluid-saturated poroelastic medium with compressible constituents[J]. **International Journal for Numerical and Analytical Methods in Geomechanics**, 2014, 38(11): 1183−1196.

[31] LI P C, WANG K Y, LU D T. Analysis of time-dependent behavior of coupled flow and deformation due to a point sink within a finite rectangular fluid-saturated poroelastic medium[J]. **Journal of Porous Media**, 2016, 19(11): 955−973.

[32] BJORCK A. Numerical methods for least squares problems[M]. Philadelphia: SIAM, 1996.

[33] NIELSEN H B. Damping Parameter in Marquardt's Method[R]. Copenhagen: Technical University of Denmark, 1999.

[34] MADSEN K, NIELSEN H B. Methods for non-linear least squares problems[R]. Copenhagen: Technical University of Denmark, 2004.

[35] DAVIS E H, RAYMOND G P. A non-linear theory of consolidation[J]. **Géotechnique**, 1965, 15(2): 161−173.

[36] GIBSON R E, ENGLAND G L, HUSSEY M J L. The theory of one-dimensional consolidation of saturated clays: 1. finite non-linear consolidation of thin homogeneous layers[J]. **Géotechnique**, 1967, 17(3): 261−273.

[37] GENG X, XU C, CAI Y. Non-linear consolidation analysis of soil with variable compressibility and permeability under cyclic loadings[J]. **International Journal for Numerical and Analytical Methods in Geomechanics**, 2006, 30(8): 803−821.

[38] STENKIN D, GORBACHENKO V. Mathematical modeling on a physics-informed radial basis function network[J]. **Mathematics**, 2024, 12(2): 241.